AD-A040 341 SOLAR SAN DIEGO CALIF F/G 11/2
STUDY OF EROSION MECHANISMS OF ENGINEERING CERAMICS.(U)
APR 77 M E GULDEN N00014-73-C-0401
UNCLASSIFIED RDR-1778-7 NL

| OF |
AD A040341

END

DATE FILMED
7-77

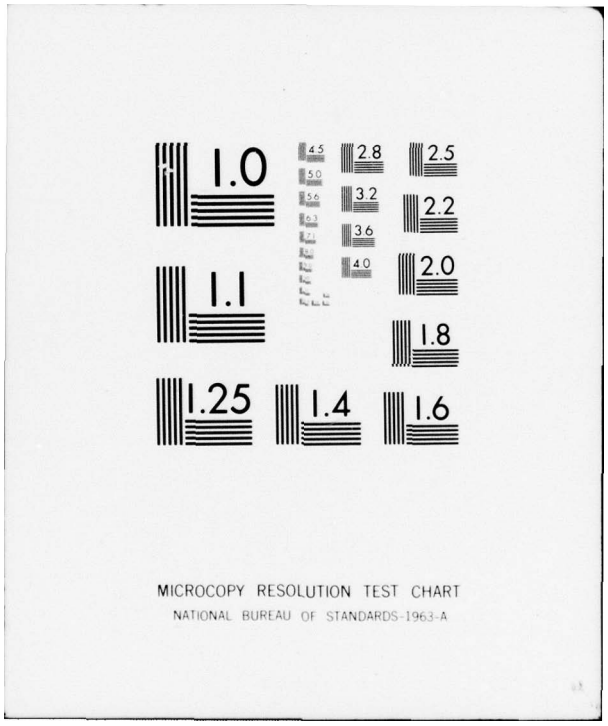
1.0
1.1
1.25
1.4
1.6
1.8
2.0
2.2
2.5
2.8
3.2
3.6
4.0
4.5
5.0
5.6
6.3
7.1
8.0
9.0
MICROCOPY RESOLUTION TEST CHART
NATIONAL BUREAU OF STANDARDS-1963-A

(12)
B.S.

April 1977

STUDY OF EROSION MECHANISMS OF ENGINEERING CERAMICS

Fifth Interim Technical Report
(January 1, 1976 to March 31, 1977

Prepared Under Contract N00014-73-C-0401
NR0-32-542

by
M. E. Gulden

for

OFFICE OF NAVAL RESEARCH
DEPARTMENT OF THE NAVY

Solar, an International
Harvester Group
San Diego, Calif

(11) April 1977 (12) 29 p.

(6)

STUDY OF EROSION MECHANISMS OF ENGINEERING CERAMICS.

Fifth Interim Technical Report
(January 1, 1976 to March 31, 1977

(9) Interim technical rept. no. 5, 1 Jan 76 - 31 Mar 77,

(15) Prepared Under Contract N00014-73-C-0401
NR0-32-542

(10) Mary Ellen by M. E. Gulden

for

OFFICE OF NAVAL RESEARCH
DEPARTMENT OF THE NAVY

Solar, an International
Harvester Group

(19) RDR-1778-7

use → 326 550

FOREWORD

This report covers the work performed by Solar from January 1, 1976 to March 31, 1977 on Contract N00014-73-C-0401 sponsored by the Office of Naval Research, Department of the Navy. Dr. A. Diness of the Metallurgy Program is monitoring this contract. The work was performed by Mary Ellen Gulden, Senior Research Engineer, as Principal Investigator under the direction of Dr. Arthur G. Metcalfe, Associate Director of Research. The testing was performed by R. Bradley Domes, Senior Research Technician.

ABSTRACT

Erosion behavior of hot pressed and reaction bonded Si_3N_4 was determined using natural quartz particles in the subsonic velocity regime. Six narrow size ranges were used varying between 15 and 385μm average diameter. Erosion behavior of these two forms of Si_3N_4 was markedly different. It was found that erosion of hot pressed Si_3N_4 was proportional to particle momentum (mass x velocity) over five orders of magnitude. Erosion of reaction bonded silicon nitride was approximately proportional to the fourth order of both particle size and velocity. Strength of hot pressed Si_3N_4 was not reduced under these test conditions. However, a major strength decrease was exhibited by the reaction bonded material. Examination revealed that erosion or impact of these materials under these test conditions did not clearly fit the current models for brittle materials, and that more than one mechanism exists. A small test program was performed on a MgF_2 target impacted with large SiC particles used as an additive in some aircraft carrier decking. It was found that cracking and material loss was sustained by the target at velocities as low as 15 mps.

TABLE OF CONTENTS

LIST OF ILLUSTRATIONS

1. INTRODUCTION

The purpose of the present program is to provide an understanding of the mechanisms of erosion of engineering ceramics and also to provide information necessary for improving erosion resistance of engineering structures. The approach is to perform experiments in a controlled manner under simulated service conditions. The target materials which have been investigated are: Alsimag 614 glass bonded Al_2O_3; NC 132 hot pressed Si_3N_4; NC 350 reaction bonded Si_3N_4; and hot pressed magnesium fluoride. All of these materials are in current use, or considered for potential use as radomes or infrared transparent windows. Silicon nitride is being considered for use in advanced gas turbine application and for bearings. Results for Alsimag 614 were presented in a previous report (Ref. 1).

The erosion tests were performed using natural quartz and SiC particles of narrow size ranges, and specific subsonic velocities. In previous work at Solar, it was found that quartz was the most erosive constituent of natural dust (Ref. 2). SiC is used as an additive in some anti-skid aircraft carrier decking.

The general approach is to determine erosion behavior and relate it to current erosion and impact models by considering particle mass-velocity dependences, appearance of massively eroded surfaces and single particle impacts, and the basic properties and structure of the targets. Erosion thresholds and effect of erosion on strength were also determined for the two forms of Si_3N_4.

2. EXPERIMENTAL PROCEDURE

2.1 EROSION TEST FACILITY AND TEST PROCEDURE

A detailed description of the erosion test facility is given in Reference 2. Briefly, erosion tests are performed with a stationary target impacted by particles accelerated in an air stream. Particles are injected into the air stream 3 meters from the target to provide sufficient distance for acceleration. High pressure, filtered and chemically dried air is used for the particle carrier gas. The carrier air velocity is measured using standard Pitot tube techniques. The air velocity variation across the 0.95 cm diameter nozzle is less than five percent and velocity is varied between 15 and 343 m/sec to achieve the desired particle velocity.

Particle velocity is measured using the rotating double disc technique described in Reference 3. Comparison with calculated velocities based on two phase flow theory is good (Ref. 1).

All erosion tests were performed at 90 degree impingement angle at ambient temperature. The number of particles used per test was varied from a few particles (to examine single particle impacts) to as many as 10^8 (to insure initiation of uniform erosion and to avoid incubation effects). The particles are fed into the gas stream using a precision feeder at a sufficiently low concentration such that particle interactions in the carrier gas stream or on the target surface are negligible. For the longtime-large number of particle tests, the specimens are weighed at specific time intervals to assess any changes in erosion with number of impacts.

Angular, high purity natural quartz particles were used for most of the erosion testing. Quartz was chosen because in previous work at Solar, it was found to the principal erosive component in natural dusts, i.e., the amount of erosion was directly proportional to the percentage of quartz in the natural dusts (Ref. 2). Six particle size ranges were used as follows: 1-30, 44-53, 62-74, 105-125, 250-297, 350-420μm. These size ranges were chosen to be representative of airborne dust and to provide significant particle mass differences of at least 1/2 order of magnitude.

The SiC particles, supplied by Bendix Abrasives Division, are used as an additive for aircraft carrier anti-skid decking. The particle size ranges from 660 to 1346μm.

2.2 STRENGTH MEASUREMENTS

Strength was determined in three point bending for both forms of Si_3N_4. Baseline values were obtained on as-received material. To determine a strength loss threshold, strength of eroded specimens was measured over a wide range of test conditions from preweight loss to massively eroded specimens. Each specimen was visually examined to insure that failure originated in the area subjected to particle bombardment. The eroded areas which are circular of 1 cm diameter were located in the center of the 2.5 or 1.25 cm specimens to insure no extraneous edge effects on strength measurements.

2.3 EXAMINATION OF ERODED SURFACES

The eroded surfaces were examined both optically, and by replica transmission and scanning electron microscopy. The progression of impact or erosion events was monitored by examining the specimens after various number of impacts for several particle size - velocity combinations ranging from single particle impacts to massively eroded surfaces. The surfaces were also examined in cross section to assess the nature of sub-surface damage.

3. EXPERIMENTAL RESULTS AND DISCUSSION

The results for the individual target materials will be discussed separately, followed by a general discussion of the implication of the results.

3.1 HOT PRESSED Si_3N_4

Most of the work was performed with NC-132 Si_3N_4 in the as-machined surface condition. This corresponds to a surface finish of ∿1μm RMS. A few specimens were polished for single particle impact evaluation.

Erosion weight loss or depth is shown as a function of number of impacts in Figure 1 for 115μ particles traveling at 219 m/sec. As can be seen, the erosion rate is linear with zero intercept except in the initial stages. Erosion in the early stages is slightly greater than expected which may be due to removal of a pre-damaged surface layer due to machining. This region corresponds to an erosion depth of ∿5μ.

3.1.1 Erosion Function of Particle Size and Velocity

Erosion weight loss as a function of particle mass and velocity was determined for conditions involving millions of particle impacts. This large number of impacts is necessary to insure that uniform erosion is occurring. Weight loss per particle was plotted versus particle radius (log - log plot) and the slopes at constant velocity were measured to determine the particle size exponent. The average value of the slope is 3.1 or mass to the first power. A similar plot of weight loss per particle versus particle velocity resulted in a velocity exponent of one. The erosion data is shown in Figure 2 plotted as a function of particle mass times velocity (particle momentum). Error bands are given for each data point. The relationship between weight loss per particle and particle momentum (mV) is valid over 5 orders of magnitude, and applies for particle sizes between 15 and 385μ and particle velocities between 24 and 285 mps. Deviations from the straight line relationship occur as the weight loss threshold is approached for 115 and 273μ particles.

This relationship between erosion weight loss and particle momentum has not been predicted by any of the models developed for erosion of brittle materials, nor has it been observed previously. The models, whether based on elastic or plastic impact response, predict a velocity exponent between 2 and 3, and a particle radius exponent near 4 (Ref. 4,5). The results do indicate that a single mechanism is controlling erosion under these test conditions.

3.1.2 Strength of Eroded Specimens

The strength of hot pressed Si_3N_4 after erosion was determined for some of the specimens used to develop Figures 1 and 2. The results are shown in Figure 3. No significant strength decrease occurred for erosion up to 37μ in depth which corresponds to 3×10^8 particle impacts or 600 grams of dust. For erosion of <1 mgm or 4μ depth, there was a trend toward strength increase, which indicates a "polishing" phenomenon may be occurring.

An estimate of the critical flaw size for the as-received material is ∿10μ using a fracture toughness value of 5 $MPa\sqrt{m}$. Since the maximum depth of

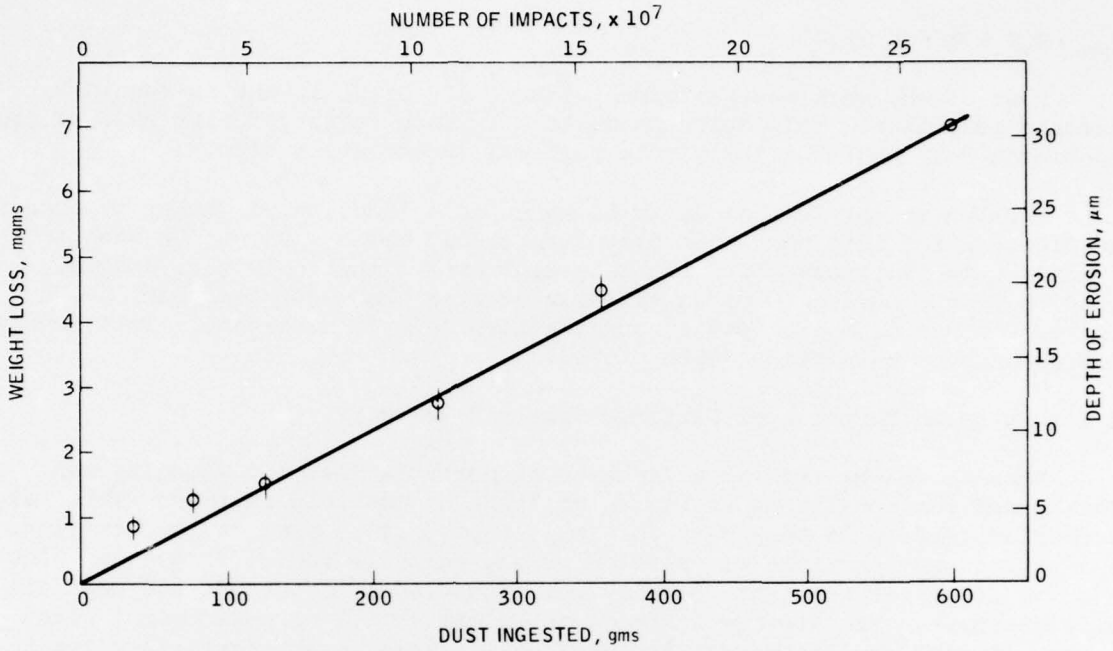

Figure 1. Erosion Weight Loss Versus Number of Impacts for Hot Pressed Si_3N_4 Impacted With 115μ Particles Traveling at 219 m/sec

erosion is ∿3X this value, the results suggest that under these erosion test conditions, the effective flaw size is no larger than pre-existing flaws characteristic of a "standard" machined surface.*

3.1.3 Examination of Eroded Surfaces

The eroded surfaces were examined optically and by electron microscopy techniques. Both single particle events and massively eroded surfaces have been viewed. The visual examination revealed that under certain erosion conditions (usually high velocities and small particles) a mosaic pattern developed on the surface. An example of this appearance is shown in Figure 4. The "matrix" regions have eroded preferentially to the "island" regions. This behavior is probably related to gross structural or compositional differences (for a given specimen, the pattern does not change with the amount of erosion, but does become more pronounced). Norton has reported that the particular batch of Si_3N_4 from which these specimens were machined does meet specifications, and in particular, is not considered to have low fracture toughness properties. They have also reported that a similar

---

* Because very large numbers of flaws are introduced by the erosion process, the effective stress concentration will depend on both size and spacing of flaws. In contrast, critical flaw sizes are calculated for isolated flaws.

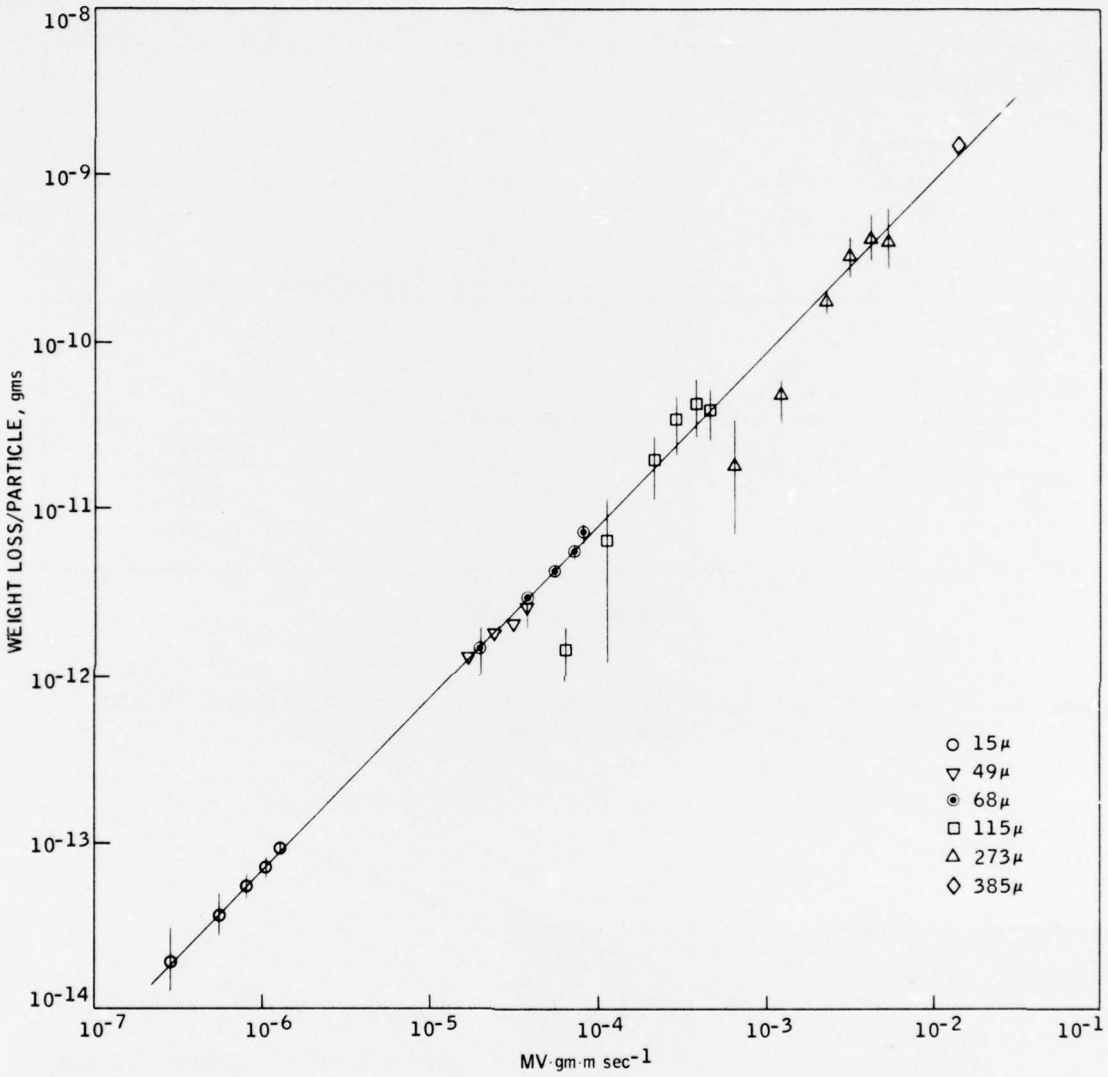

Figure 2. Erosion Weight Loss per Particle Versus a Measure of Particle Momentum for Hot Pressed Si_3N_4 in the Uniform Erosion Range. Quartz Particles - Velocity Varied Between 24 and 285 mps.

pattern develops under some etching and polishing conditions. These surfaces were examined using scanning electron microscopy with an energy dispersive X-ray attachment in an attempt to identify differences in composition, particularly trace elements. The following elements were examined: Na, Mg, Al, Si, K, Ca, Fe and W. No differences in composition were detected, and except for Si, the number of counts was low.

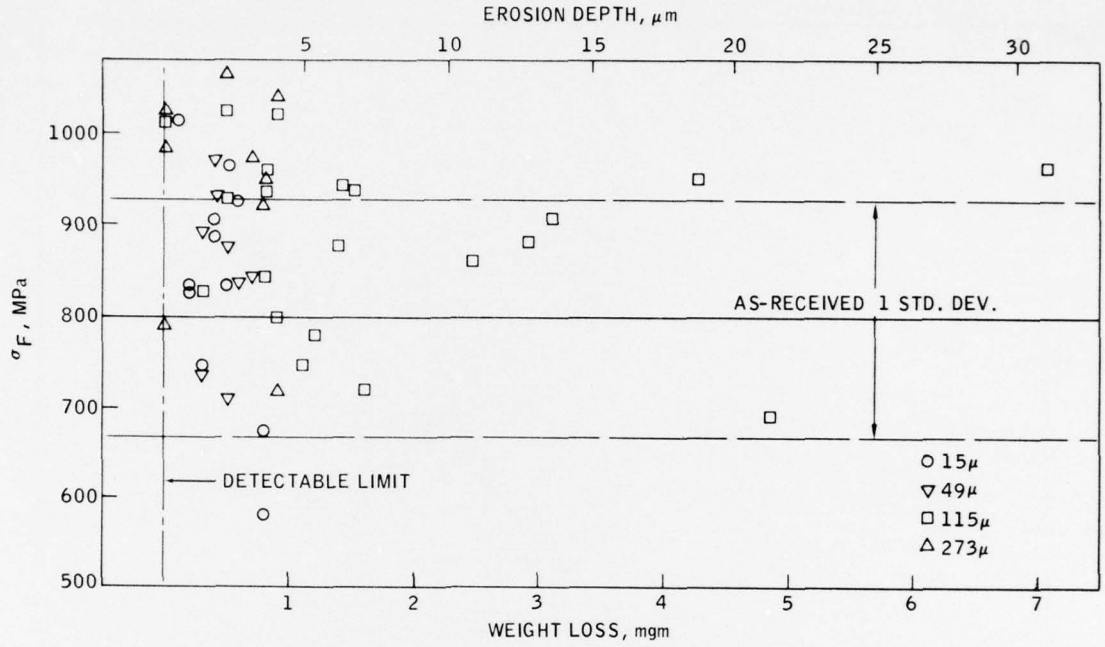

Figure 3. Effect of Erosion on Strength of Hot Pressed Si_3N_4. Erosion conditions are the same as those of Figure 1.

Figure 4.

Surface of Hot Pressed Si_3N_4 Showing Nonuniform Erosion

2×10^8 Particles
115μ Diameter
219 m/s Velocity

Magnification: 10X

Examination of the eroded surfaces by electron microscopy has not been particularly instructive. In the case of single particle events, the impact areas are not differentiable from the as-machined ground surface, an example of which is shown in Figure 5. The heavily eroded surfaces (Fig. 6) generally have a relatively flat featureless appearance and do not provide information concerning possible mechanisms. A limited number of tests have been performed on polished surfaces and provide more information concerning particle impact response. Damage from a single 273μ quartz particle traveling at 188 m/sec is shown in Figure 7. The chip which has been removed (∿4μ dia) is quite small compared with the predicted contact area based on elastic impact of a spherical particle (∿50μ dia.) and no secondary cracking is apparent. This type of damage, which is typical under these test conditions, is not characteristic of classical elastic or plastic impact response.

An estimate of the volume of material removed per impact can be made from the weight loss data on heavily eroded surfaces. If it is assumed that the shape is a half sphere, the radius of this sphere is 4μ for 273μ particles traveling at 188 m/sec. This compares with a measured radius of ∿2μ (Fig. 7). Considering the statistical nature of the calculations and the test procedure, this shows quite good agreement between single particle impacts and bulk erosion, and suggests that secondary cracking and residual erosion damage do not play a significant role in the erosion process under these test conditions.

The eroded specimens were examined in cross section to assess the extent of subsurface damage. The structure under the eroded area was indistinguishable from that below the as-machined surface, and subsurface cracking was not apparent. This observation is consistent with the strength measurements.

3.2 REACTION BONDED Si_3N_4

NC-350 reaction bonded Si_3N_4 was subjected to the same erosion conditions discussed previously for hot pressed Si_3N_4. The material was tested in two conditions termed "as-fired" and "polished." The as-fired material contains the oxide surface layer inherent in this type of processing. In the polished condition, this surface layer was removed.

3.2.1 Erosion Function of Particle Size and Velocity

It was found that the oxide surface layer erodes more rapidly than the bulk material. A characteristic example of this behavior is shown in Figure 8. Beyond the surface layer, the erosion rates for as-fired and polished material are the same as would be expected. Although not shown in Figure 9, the depth of material showing the increased erosion rate is ∿100μ. Visually, the grey surface layer is ∿50μ thick. Apparently, the extent of surface compositional and structural differences extends deeper into the material than appears visually.

Figure 5.

As-Received Ground Surface of Hot Pressed Si_3N_4

Magnification: 8000X
(TEM-Replica)

Figure 6.

Eroded Surface of Hot Pressed Si_3N_4

3.4×10^7 Particles
115μ Diameter
219 m/s Velocity
Depth of Erosion ≅4.5μ

Magnification: 8000X
(TEM-Replica)

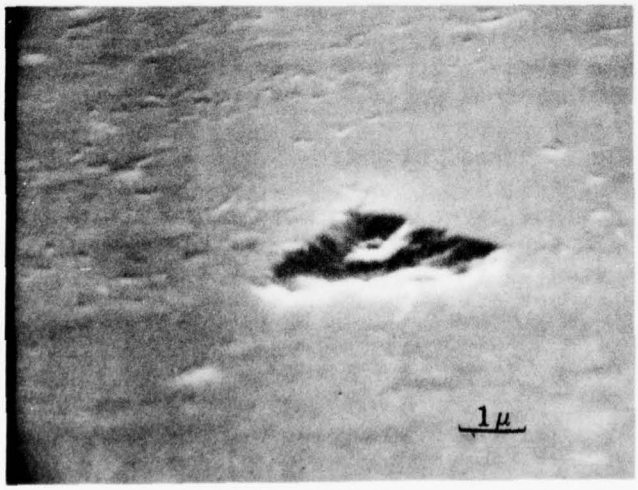

Figure 7.

Single Particle Impact on Polished Hot Pressed Si_3N_4 Surface

273μ Quartz
188 m/s Velocity
Average Contact Radius ≅25μ

Magnification: 10,000X

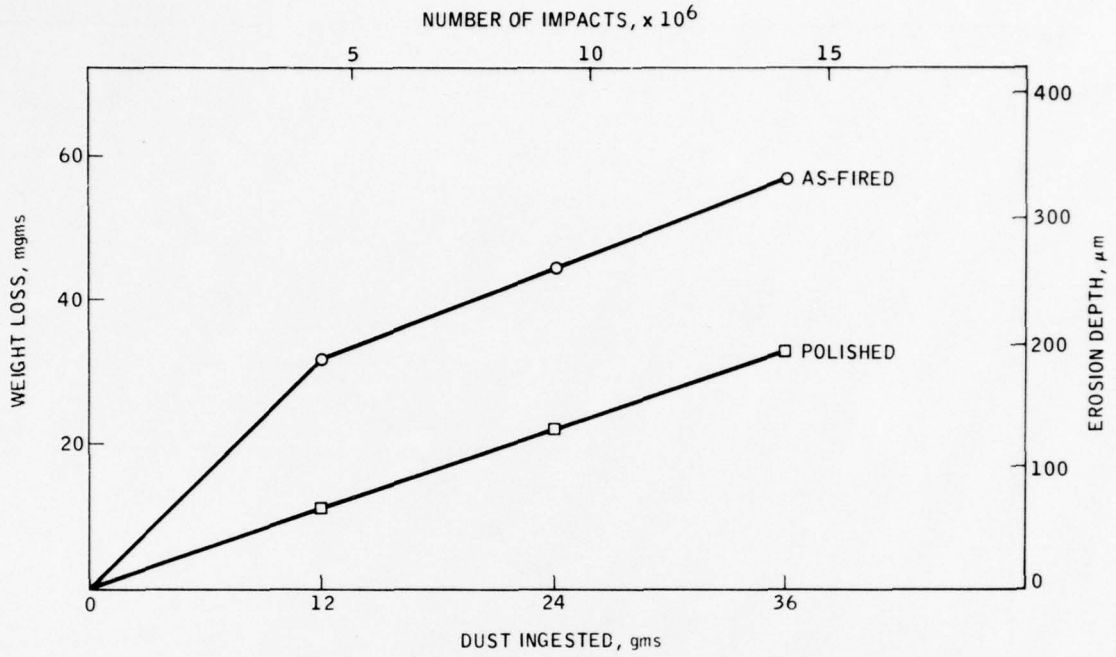

Figure 8. Effect of Surface Layer on Erosion of Reaction Bonded Si_3N_4. As-fired Condition Contains Surface Oxide Layer. Polished Condition has Layer Removed. (273μ Quartz, 155 mps).

The function of particle size and velocity on erosion of reaction bonded Si_3N_4 was established with polished specimens. Weight loss per particle was plotted versus particle radius (log-log plot) and the slopes at constant velocity were measured to determine the particle size or mass exponent. The average value of the slope was close to 4. A similar plot of weight loss per particle versus particle velocity resulted in a particle radius exponent of 4 also. The erosion data is shown plotted as a function of particle radius and velocity to the fourth power in Figure 9. The weight loss thresholds are indicated by arrows. The data are fairly consistent with this function except for 15μ particles, but the error in assumption of a mean radius of 15μ for the 1 to 30 micron fraction is very large for this fraction.

For all particle sizes, a measurable weight gain occurred at the lower velocities which indicates particles are embedding in the surface. For the 15μ particles, this occurred at a velocity as high as 175 m/sec. Although measurable weight loss occurred at higher velocities for this particle size, it is possible that particles are embedding at all velocities, which would explain the deviation from $(RV)^4$ function shown in Figure 10 for the 15μ particles.

A measurable weight gain has not been experienced with the other ceramic target materials investigated on this program. However, reaction bonded Si_3N_4 is the only material that is not fully dense and contains appreciable porosity. Based on a comparison of densities, the porosity is on the order of 25 percent.

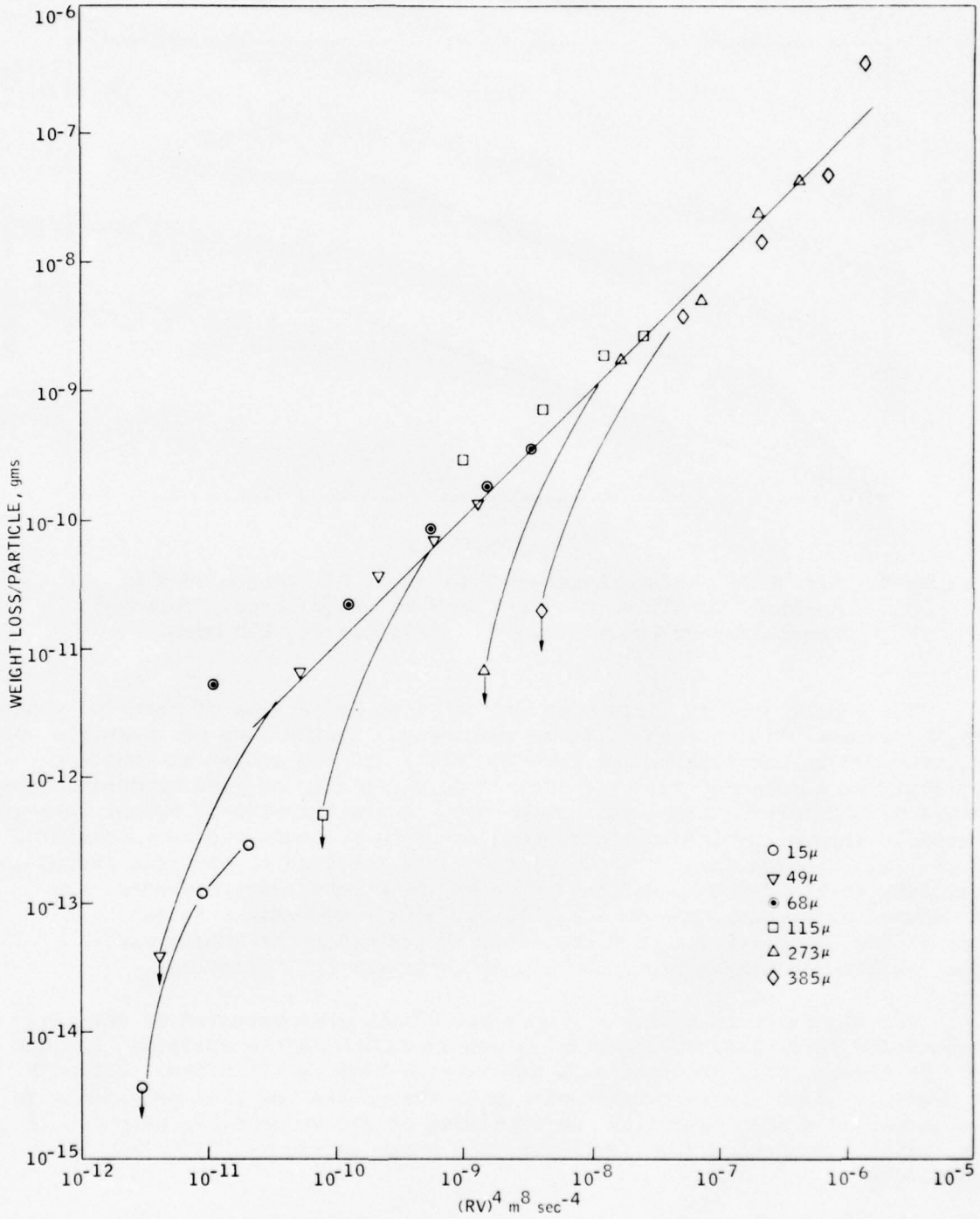

Figure 9. Erosion Weight Loss Per Particle Versus $(RV)^4$ for Reaction Bonded Si_3N_4 in Uniform Erosion Range. Quartz Particles - Velocity Varied Between 40 and 285 mps.

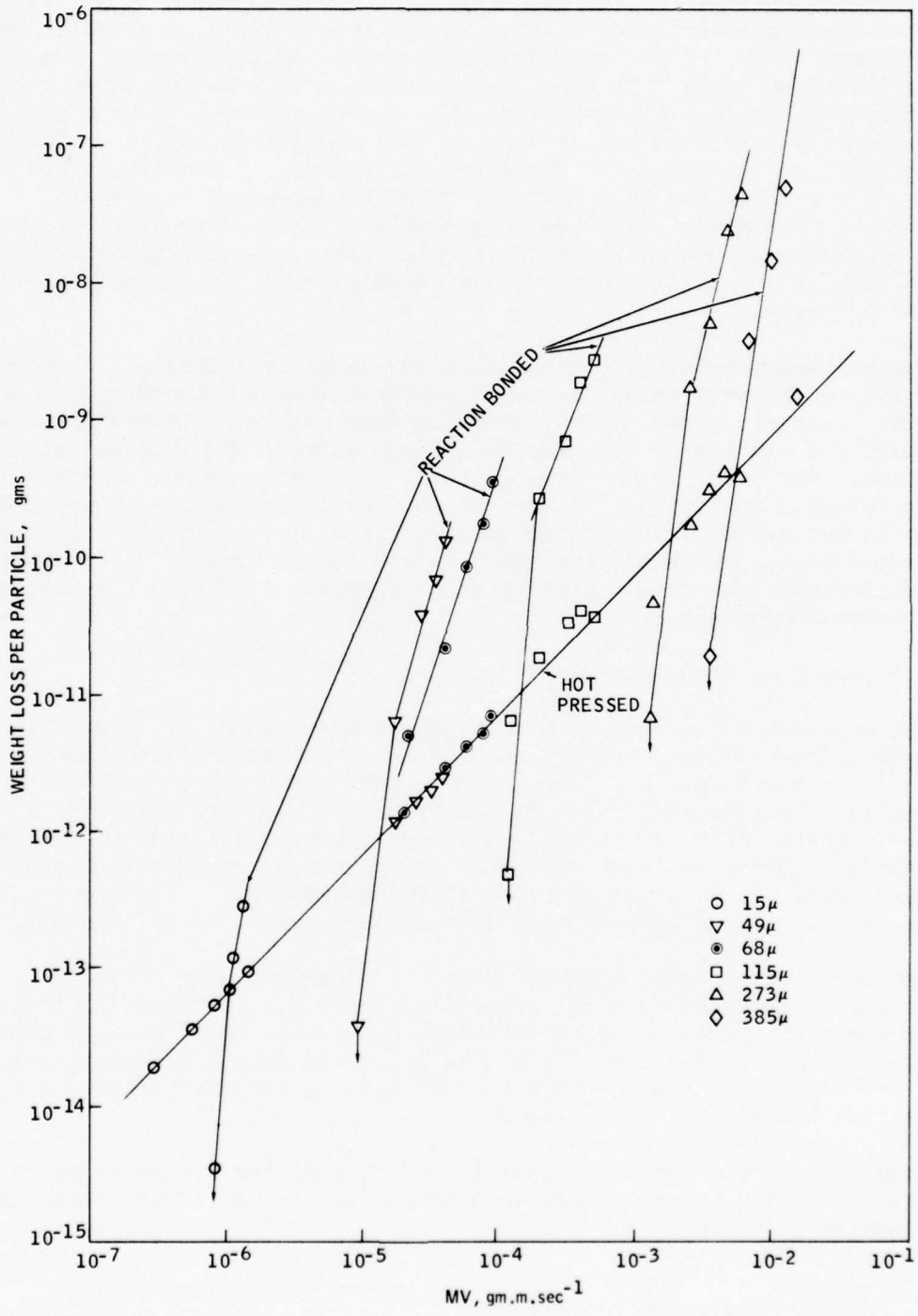

Figure 10. Erosion Weight Loss Versus Particle Momentum

The dependence of erosion on particle size to the fourth power is predicted by both elastic and plastic impact models (Refs. 4 and 5). The radius exponent for the referenced elastic impact models results from a combination of Hertzian type impact and Weibull statistics which includes a size effect due to flaw distribution. The radius exponent for the plastic impact model results from the assumption that erosion or material removal is due primarily to lateral crack formation and growth. However, neither of these models predict the high particle velocity dependence on erosion exhibited by this material. This is probably related to the fact that the models generally assume an isotropic single phase material whereas reaction bonded Si_3N_4 is essentially a two-phase material with the second phase being composed of pores.

The extreme sensitivity on erosion with velocity increases is shown in Figure 10, which gives weight loss per particle versus a function of particle momentum. Particle momentum was chosen because of the relationship shown previously for erosion of hot pressed silicon nitride under identical test conditions. The data for hot pressed Si_3N_4 are also included. Under the highest velocity conditions, erosion weight loss of reaction bonded Si_3N_4 is as much as two orders of magnitude greater for a given particle size than for hot pressed Si_3N_4, but under low velocity conditions erosion weight loss is still occurring with the hot pressed material while a weight gain occurs with the reaction bonded material.

3.2.2 Strength of Eroded Specimens

The strength of reaction bonded Si_3N_4 after erosion was determined for specimens in the as-fired surface conditions. The results are shown in Figure 11. Several specimens were also tested in the as-received condition to establish baseline strength. If the specimens had been polished, a higher average strength would be expected, but previous work at Solar has shown a much greater scatter in strength values for polished compared with as-fired specimens (Ref. 6). For values up to $\sim$100μ erosion depth, surface layer effects exist. Beyond 100μ, the results reflect parent material behavior.

Specimens were eroded with the particle sizes shown in Figure 11 traveling at various velocities. There is an obvious decrease in strength with erosion. An estimate of the critical flaw size, based on a fracture toughness value of 2.2 MPa $m^{1/2}$ gives $\sim$17μ for the as-received material, and $\sim$230μ for the weakest eroded specimen, which is an increase of over 1 order of magnitude in critical flaw size.

According to the model for plastic impact response discussed previously, the strength of the target should be dominated by radial crack formation by the following relation:

$$\sigma_F \alpha \frac{K_{iC}}{V^{0.5} R^{0.8}} \qquad \text{(Ref. 5).}$$

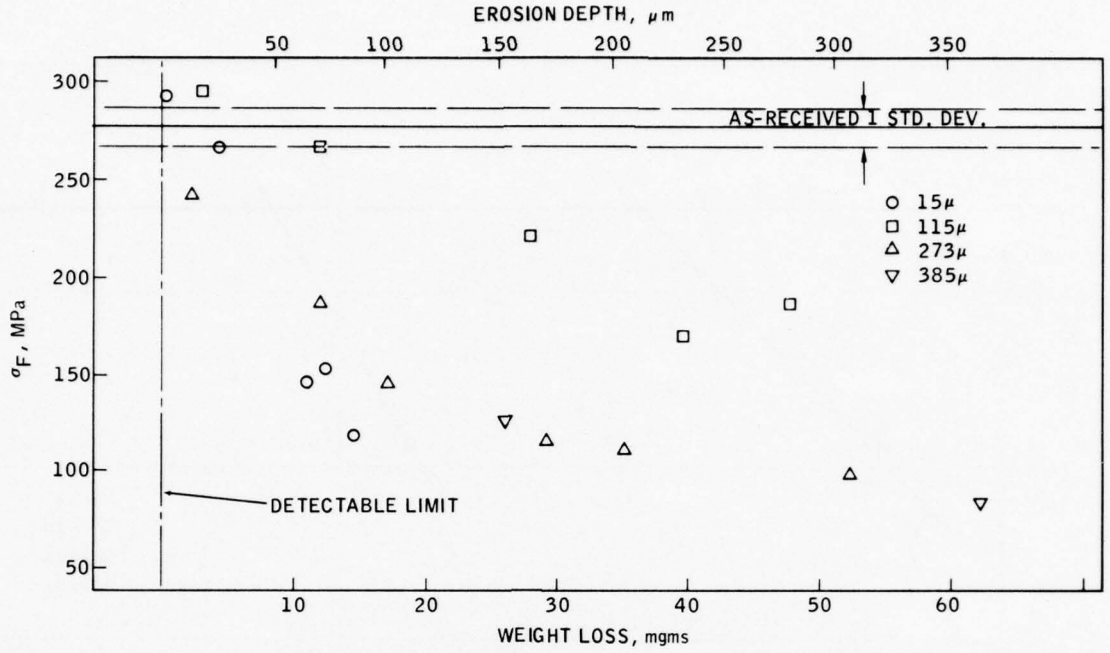

Figure 11. Effect of Erosion on Strength of Reaction Bonded Si_3N_4

A plot of strength versus $(V^{0.5}R^{0.8})^1$ is shown in Figure 12. The data falls roughly into two groups which both have slopes close to 1 on a log-log basis. The major difference between these two groups is particle size and depth of erosion. The depth of erosion for these particular specimens subjected to 15μ particle bombardment was still within the surface layer which has different material properties and composition than the bulk material.

It is also possible that the type of damage produced with the 15μ particles differs from that produced with the larger particles. As discussed previously, the erosion weight loss values for 15μ particles was not consistent with the $(RV)^4$ function of the larger particles.

3.2.3 Examination of Eroded Surfaces

The eroded surfaces were examined using scanning electron microscopy and standard metallographic techniques. Single impacts were characterized by relatively deep pits with no apparent evidence of secondary cracks intersecting the surface. An example is shown in Figure 13 for impact with a 385μ particle traveling at 174 mps. The approximate contact radius was calculated to be 35μ based on spherical elastic impact. The radius of the impact crater is very close to this value. An estimate of the volume of material removed per impact can be made from the weight loss data on heavily eroded surfaces. If it is assumed that the shape is a half sphere, the radius of this sphere is 41μ which is in good agreement with the size of the impact crater shown in Figure 13. This agreement indicates that secondary cracking and residual erosion damage do not play a significant role in erosion weight loss under these test conditions, i.e., the amount of material removed per impact for the first impact is approximately the same as for the

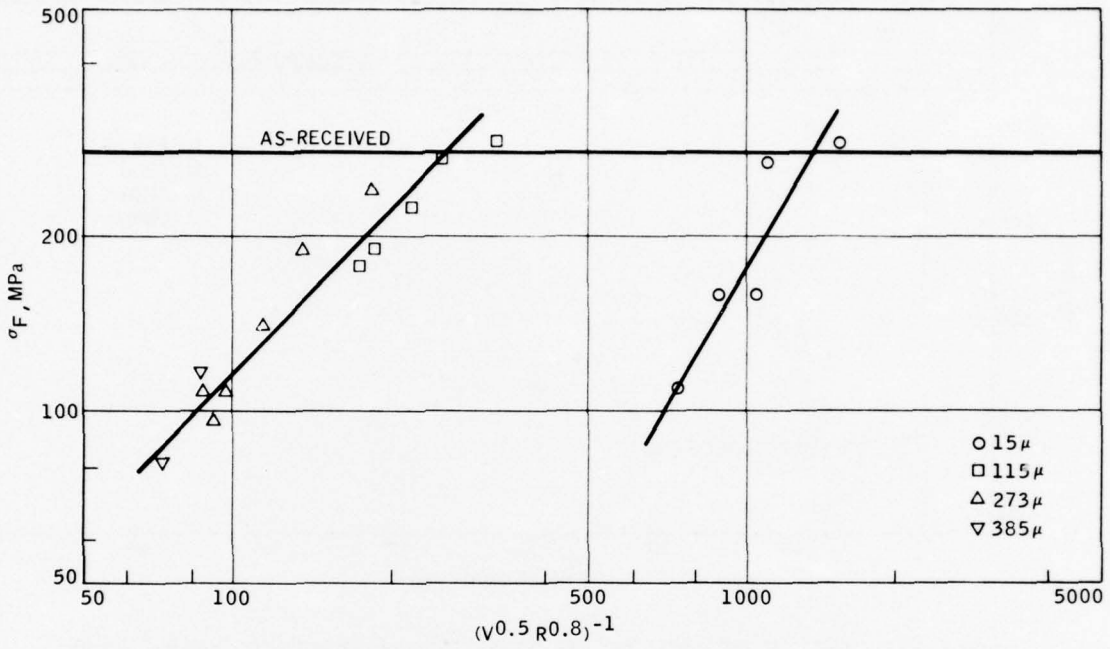

Figure 12. Strength Versus Function of Predicted Radial Crack Formation for Reaction Sintered Si_3N_4

Figure 13. Single Particle Impact on Reaction Bonded Si_3N_4. 385μ Quartz 174 mps Velocity. Average Contact Radius ∿35μ. Magnification: 500X

millionth impact. This observation applies for conditions after removal of the surface oxide layer. This type of damage was characteristic of all particle sizes (except 15μ) and velocities. As expected, absolute size and depth of the impact damage varied with particle velocity and size. For the smallest particles (15μ) single impacts could not be differentiated from the porosity inherent to reaction bonded Si_3N_4.

A selection of the eroded surfaces was examined in cross section to assess the extent of subsurface damage. Two examples are shown in Figure 14. The depth of the secondary cracks in Figure 14a is ∿180μ which is consistent with the calculated critical flaw size based on strength of this specimen. The direction of the subsurface cracks is consistent with an increased flaw size. Very little evidence of lateral cracking was observed for the conditions of Figure 14a. The subsurface damage produced with the much smaller 15μ particles is apparently different in type (Fig. 14b) than that produced with 385μ particles. No evidence of appreciable radial cracks (perpendicular to surface) was observed, and shallow lateral cracks were present. The depth of these cracks was ∿30μ. Lateral cracks are expected to influence strength less than radial cracks. The calculated critical flaw size for this specimen was ∿90μ. The explanation for this apparent discrepancy between the size of subsurface cracks and calculated flaw size is not apparent.

3.3 MAGNESIUM FLUORIDE

The purpose of this phase of the investigation was to determine the extent and type of damage produced by coarse SiC particles on a MgF_2 target (Irtran I, produced by Kodak). The particles, obtained from Abrasive Division, Bendix Corporation, are those used in some aircraft carrier decking. The particles are irregularly shaped and angular as shown in Figure 15. The particle size ranges between 660 and 1346μ. Tests were performed at 6 velocities (125, 104, 81, 37, 30 and 15 mps) considered characteristic of conditions created during take-off and landing of aircraft on a deck surface impregnated with these particles. Since damage was expected to be extensive, only 6 particles per test were used. Damage was sustained by the MgF_2 under all test conditions. Examples are shown in Figure 16. A typical SiC particle is included to illustrate relative size of damage produced and material removed. Plastic impact response was observed for all velocities. Plastic impact response is characterized by fracture propagating from the plastically deformed contact area. The two types of fracture are radial cracks which propagate radially outward from the contact zone, and lateral cracks that initiate under the contact zone and propagate on planes nearly parallel to the surface. Material removal occurred primarily by loss of the volume bounded by the lateral cracks. For particles traveling at higher velocities, the magnitude of damage or loss produced by a single particle impact is of the same order as the particle size. At the higher velocities small chips were also seen, which presumably, were secondary damage produced by fragments from the initial impact.

a) 385μ Particles
174 mps Velocity
Erosion Depth = 375μ
Crack = 180μ

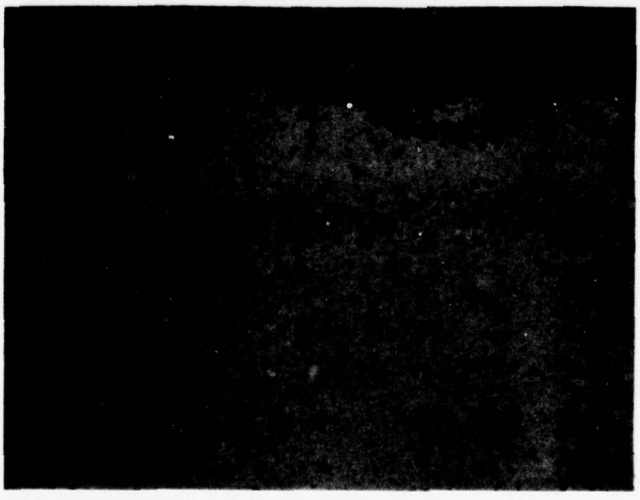

b) 15μ Particles
285 mps Velocity
Erosion Depth = 90μ
Crack = 30μ

Figure 14. Cross Section of Heavily Eroded Reaction Bonded Si_3N_4. Arrows indicate Extent of Subsurface Cracking. Magnification: 250X

Figure 15. SiC Particles Used for Eroding MgF_2 Magnification: 14X

It was also observed that a single particle could produce more than one distinct area of damage. An example is shown in Figure 17. Apparently the particles are sufficiently angular to impact the target at more than one point. If this type of single particle damage is appreciable, it could lead to errors in predicting gross erosion behavior from the size and shape of individual damaged regions, particularly under idealized conditions. In the current case, since only 6 particles were used for each test, and these particles impacted on an area of 0.7 cm^2, the damage produced by each particle could be identified. The relative importance of this type of phenomenon will be dependent on particle type and shape.

3.4 GENERAL DISCUSSION

To this point, the results for each target material have been discussed separately. In this section a comparision will be made between the erosion behavior of the various target materials, and the results will be discussed in terms of impact models and materials properties and structure.

During the course of this program four engineering ceramics have been subjected to erosion conditions considered characteristic of a natural dust environment. Under these conditions, the erosion response differs markedly as shown in Figure 18. For a given erosion condition, there is approximately 1 order of magnitude difference in erosion weight loss between each of the targets. There is also considerable variation in material properties and structure between the targets. Table 1 lists the physical properties considered relevant to erosion response. Of the properties listed, fracture toughness is the only property which varied consistently with erosion. The other properties (elastic modulus and hardness) would predict either less separation in erosion weight loss or a different ranking of erosion resistance. The effect of structure and particle type on erosion will be discussed later.

126 m/sec Velocity
2 Impacts

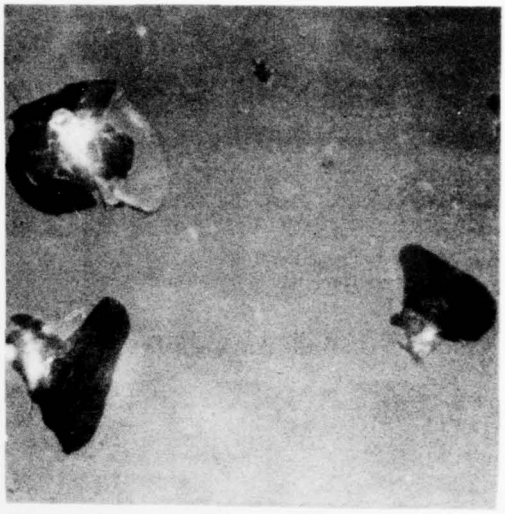

30 m/sec Velocity
3 Impacts

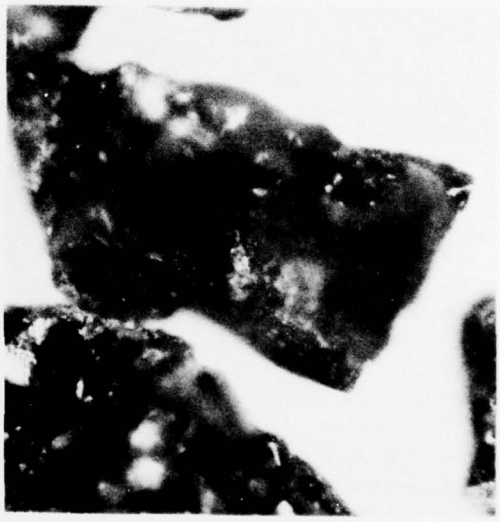

Typical Particle

Figure 16. Erosion of MgF_2 by SiC Particles. Magnification: 40X

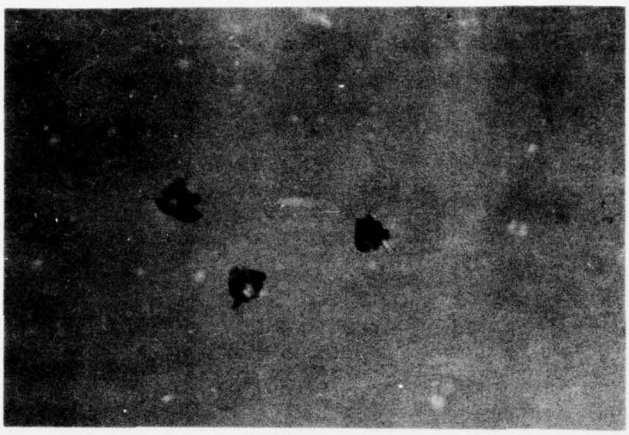

Figure 17.

Damage Produced by Single Particle Impact on MgF_2 Target

Magnification: 40X

To date, essentially two types of models have been proposed for impact or erosion of brittle materials (Refs 4 and 5). The earlier models were based on elastic interaction and predicted that material removal occurs by the intersection of ring cracks on the substrate surface. This process has been observed on glass impacted with glass spheres (Ref. 7) but was not observed with these target materials under these test conditions. More recent analysis has treated static and dynamic plastic indentation which is characterized by plastic deformation of the contact area between the particle and the target, radial cracks propagating outward from the contact zone, and lateral cracks that initiate beneath the contact zone and propagate between the radial cracks on planes nearly parallel to the surface. The former are considered a source of strength degradation, and the latter a potential source of material removal (Ref. 5).

Based on the plastic impact model, maximum erosion loss per impact would be proportional to the volume encompassed by the lateral cracks which results in the following expression (Ref. 5).

$$E \simeq V^{2.5} R_p^{4} \rho_p^{0.3} (1/HK_c^{5})^{0.3} f(M)$$

where E = volume removed per impact

V = particle velocity

R_p = particle radius

ρ_p = particle density

H = target hardness

K_c = target fracture toughness

$f(M)$ = is the fraction of the volume encompassed by the lateral cracks that is actually removed and is considered a material dependent variable.

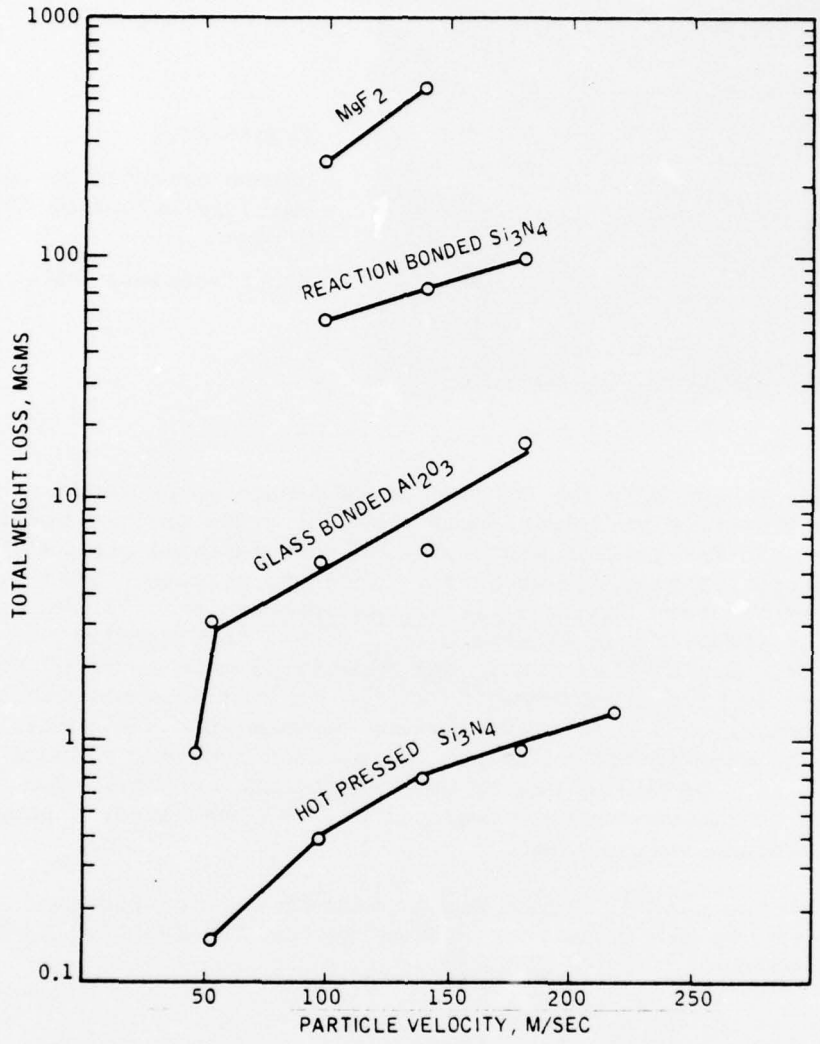

Figure 18. Erosion Weight Loss Comparison
2×10^7 Particles of 115μ Quartz

Table 1

Physical Properties of Target Materials and Particles

	Elastic Modulus G Pa	Fracture Toughness MPa $m^{1/2}$	Hardness* G Pa	Structure
Hot Pressed Si_3N_4 (NC-132)	320	5.0	16	Pseudo single phase 2μ grain size
Glass Bonded Al_2O_3 (Alsimag 614)	324	4	12	Two phase 4% glass - 96% Al_2O_3 10μ grain size
Reaction Bonded Si_3N_4 (NC-350)	170	2.2	3	Multi phase - Si_3N_4+ porosity + Si + SiO_2 (surface)
Hot Pressed MgF_2 (Irtran L)	170	1	6	Single phase ∿2μ grain size
Natural Quartz	95	∿0.7	∿6	

* The hardnesses are the quasi-static Vickers hardness in the macro indentation load independent regime.

Using the data from Figure 18, this relationship does predict the relative erosion rank of the four target materials. However, a log-log plot of erosion/$V^{2.5}$ versus ($1/Kc^5H$) results in a slope of ∿0.6 between Al_2O_3, RB Si_3N_4 and MgF_2 compared to the predicted value of 0.3 (Ref. 5). The erosion data for hot pressed Si_3N_4 does not follow the straight line relationship of the other materials, but shows a reduced erosion rate. Furthermore, the velocity exponent of 2.5 does not provide good normalization of the erosion data between erosion and material properties.

These apparent discrepancies between predicted erosion from plastic impact and observed erosion for these four ceramics can be related in part to structural differences, and also to the appearance of the impact damage. The model assumes an isotropic material. Hot pressed Si_3N_4 under these test conditions exhibits very minor chipping, and it is considered to be below the plastic impact response threshold. However, plastic impact does occur with hot pressed Si_3N_4 impacted with 200μ WC particles traveling at 650 mps (Ref. 5). The other three targets exhibited plastic impact, but MgF_2 was the only material showing extensive lateral crack formation. Glass bonded Al_2O_3 and reaction bonded Si_3N_4 are two-phase materials, and at least with the Al_2O_3, erosion is a two-phase process as well (Ref. 1). The glass grain boundary phase, which can be as wide as 3μ eroded preferentially to the alumina

grains. In extreme cases, no apparent damage was sustained by the grains, and erosion occurred by actual grain fallout after extensive grain boundary erosion. Since reaction bonded silicon nitride contains ~25% porosity, a crushing phenomenon probably contributes to the erosion process which would be absent in a fully dense material. As seen in Figure 14a, subsurface cracking appears to propagate between pores. Also, a weight gain, ostensibly due to particle embedment in the pores, was observed with reaction bonded Si_3N_4.

As mentioned previously, the particle composition and shape is known to affect type of erosion response. However, since the intent of this program was to simulate a natural dust environment, particle variables other than size and velocity have not been considered.

These points are presented to illustrate the fact that erosion of "engineering" ceramics under a simulated dust environment can be a complex process, and more than one mechanism exists for this group of materials under identical erosion conditions.

4. SUMMARY

Solid particle erosion response of hot pressed and reaction bonded Si_3N_4 was determined under conditions which simulate a service dust environment, i.e., natural quartz particles at subsonic velocities.

It was found that erosion weight loss per particle for hot pressed Si_3N_4 was proportional to particle momentum (particle mass x velocity) over 5 orders of magnitude, and that strength was not reduced by erosion under these test conditions.

Erosion weight loss for reaction bonded Si_3N_4 showed a much higher dependence on particle velocity in the approximate proportion of R^4V^4. A marked strength reduction was also observed. A weight gain was observed under low velocity conditions.

Examination of single impacts revealed that erosion of hot pressed Si_3N_4 occurs by minor chipping where the approximate diameter of the material removed is one order of magnitude less than the estimated contact diameter. The diameter of material removed per impact for reaction bonded Si_3N_4 was essentially the same as the estimated particle contact diameter. In both cases, secondary cracking was not observed on the surface. However, reaction bonded Si_3N_4 exhibited extensive subsurface radial cracks.

Magnesium fluoride impacted with SiC particles used in aircraft carrier decking exhibited damage at velocities as low as 15 mps.

It was concluded that more than one mechanism of erosion exists under "natural" dust environments, and that the mechanisms are dependent not only on target physical properties, but also to a large extent on structure.

REFERENCES

1. Gulden, M.E. and Metcalfe, A.G., Study of Erosion Mechanisms of Engineering Ceramics, Solar Report RDR 1778-4, Contract N00014-73-C-0401, (1976).

2. Smeltzer, C.E., Gulden, M.E., McElmury, S.S. and Compton, W.A., Mechanisms of Sand and Dust Erosion in Gas Turbine Engines, USAAVLABS Tech. Report 70-36 (1970).

3. Ruff, A.W. and Ives, L.K., Wear, 35 pg. 195, (1975).

4. Oh, H.L., Oh, K.D.L., Vaidyanathan, S. and Finnie, I., On the Shaping of Brittle Solids by Erosion and Ultrasonic Cutting, NBS Special Publication 348, pg. 119, (1972).

5. Evans, A.G., Gulden, M.E., Eggum, G.E. and Rosenblatt, M., Impact Damage in Brittle Materials in the Plastic Response Regime, Contract N00014-75-C-0669, Report No. SC5023.9TR, (1976).

6. Gulden, M.E. and Metcalfe, A.G., J. Am. Cer. Soc, 59, pg 391, (1976).

7. Adler, W.F., Analysis of Multiple Particle Impacts on Brittle Materials, AFML Tech. Report 74-210, (1974).

BASIC DISTRIBUTION LIST October 1976

Technical and Summary Reports

Organization	No. of Copies
Defense Documentation Center Cameron Station Alexandria, Virginia 22314	(12)
Office of Naval Research Department of the Navy	
Attn: Code 471	(1)
Code 102	(1)
Code 470	(1)
Commanding Officer Office of Naval Research Branch Office 495 Summer Street Boston, Massachusetts 02210	(1)
Commanding Officer Office of Naval Research Branch Office 536 South Clark Street Chicago, Illinois 60605	(1)
Office of Naval Research San Francisco Area Office 760 Market Street, Room 447 San Francisco, California 94102 Attn: Dr. P. A. Miller	(1)
Naval Research Laboratory Washington, D.C. 20390	
Attn: Code 6000	(1)
Code 6100	(1)
Code 6300	(1)
Code 6400	(1)
Code 2627	(1)
Naval Air Development Center Code 302 Warminster, Pennsylvania 18974 Attn: Mr. F. S. Williams	(1)
Naval Air Propulsion Test Center Trenton, New Jersey 08628 Attn: Library	(1)

Organization	No. of Copies
Naval Construction Batallion Civil Engineering Laboratory Port Hueneme, California 93043 Attn: Materials Division	(1)
Naval Electronics Laboratory Center San Diego, California 92152 Attn: Electron Materials Sciences Division	(1)
Naval Missile Center Materials Consultant Code 3312-1 Point Mugu, California 93041	(1)
Commanding Officer Naval Surface Weapons Center White Oak Laboratory Silver Spring, Maryland 20910 Attn: Library	(1)
David W. Taylor Naval Ship R&D Center Materials Department Annapolis, Maryland 21402	(1)
Naval Undersea Center San Diego, California 92132 Attn: Library	(1)
Naval Underwater System Center Newport, Rhode Island 02840 Attn: Library	(1)
Naval Weapons Center China Lake, California 93555 Attn: Library	(1)
Naval Postgraduate School Monterey, California 93940 Attn: Mechanical Engineering Dept.	(1)
Naval Air Systems Command Washington, D.C. 20360	
Attn: Code 52031	(1)
Code 52032	(1)
Code 320	(1)

Organization	No. of Copies
Naval Sea System Command Washington, D.C. 20362 Attn: Code 035	(1)
Naval Facilities Engineering Command Alexandria, Virginia 22331 Attn: Code 03	(1)
Scientific Advisor Commandant of the Marine Corps Washington, D.C. 20380 Attn: Code AX	(1)
Naval Ship Engineering Center Department of the Navy CTR BG #2 3700 East-West Highway Prince Georges Plaza Hyattsville, Maryland 20782 Attn: Engineering Materials and Services Office, Code 6101	(1)
Army Research Office Box CM, Duke Station Durham, North Carolina 27706 Attn: Metallurgy & Ceramics Div.	(1)
Army Materials and Mechanics Research Center Watertown, Massachusetts 02172 Attn: Res. Programs Office (AMXMR-P)	(1)
Air Force Office of Scientific Research Bldg. 410 Bolling Air Force Base Washington, D.C. 20332 Attn: Chemical Science Directorate Electronics and Solid State Sciences Directorate	(1) (1)
Air Force Materials Lab (LA) Wright-Patterson AFB Dayton, Ohio 45433	(1)

Organization	No. of Copies
NASA Headquarters Washington, D.C. 20546 Attn: Code RRM	(1)
NASA Lewis Research Center 21000 Brookpark Road Cleveland, Ohio 44135 Attn: Library	(1)
National Bureau of Standards Washington, D.C. 20234 Attn: Metallurgy Division Inorganic Materials Division	(1) (1)
Defense Metals and Ceramics Information Center Battelle Memorial Institute 505 King Avenue Columbus, Ohio 43201	(1)
Director Ordnance Research Laboratory P.O. Box 30 State College, Pennsylvania 16801	(1)
Director Applied Physics Laboratory University of Washington 1013 Northeast Fortieth Street Seattle, Washington 98105	(1)
Metals and Ceramics Division Oak Ridge National Laboratory P.O. Box X Oak Ridge, Tennessee 37380	(1)
Los Alamos Scientific Laboratory P.O. Box 1663 Los Alamos, New Mexico 87544 Attn: Report Librarian	(1)
Argonne National Laboratory Metallurgy Division P.O. Box 229 Lemont, Illinois 60439	(1)

Organization	No. of Copies	Organization	No. of Copies
Brookhaven National Laboratory Technical Information Division Upton, Long Island New York 11973 Attn: Research Library	(1)		
Library Building 50 Room 134 Lawrence Radiation Laboratory Berkeley, California	(1)		

ER
October 1976

SUPPLEMENTARY DISTRIBUTION LIST

Technical and Summary Reports

Dr. W. F. Adler
Effects Technology Inc.
5383 Hollister Avenue
P.O. Box 30400
Santa Barbara, CA 92105

Dr. G. Bansal
Battelle
505 King Avenue
Columbus, OH 43201

Dr. S. A. Bortz
IITRI
10 W. 35th Street
Chicago, IL 60616

Dr. J. D. Buch
Prototype Development Assoc., Inc.
1740 Garry Avenue, Suite 201
Santa Ana, CA 92705

Dr. B. Budiansky
Harvard University
Department of Engineering and
Applied Science
Cambridge, MA 02138

Professor.H. Conrad
University of Kentucky
Materials Department
Lexington, KY 40506

Dr. A. Cooper
Case Western Reserve University
Materials Department
Cleveland, OH 44106

Dr. N. Corney
Ministry of Defence
The Adelphi
John Adam Street
London WC2N 6BB
UNITED KINGDOM

Dr. A. G. Evans
Rockwell International
P.O. Box 1085
1049 Camino Dos Rios
Thousand Oaks, CA 91360

Professor John Field
University of Cambridge
New Cavendish Laboraotry
Cambridge,
UNITED KINGDOM

Dr. I. Finney
University of California
Berkeley, CA 94720

Mr. A. A. Fyall
Royal Aircraft Establishment
Farnborough, Hants
UNITED KINGDOM

Dr. L. M. Gillin
Aeronautical Research Laboratory
P.O. Box 4331
Fisherman's Bend
Melbourne, VIC 3001
AUSTRALIA

Dr. M. E. Gulden
International Harvester Company
Solar Division
2200 Pacific Highway
San Diego, CA 92138

Professor. A. H. Heuer
Case Western Reserve University
University Circle
Cleveland, OH 44106

Dr. R. Hoagland
Battelle
505 King Avenue
Columbus, OH 43201

SUPPLEMENTARY DISTRIBUTION LIST (Cont'd)

Dr. R. Jaffee
Electric Power Research
Institute
Palo Alto, CA

Dr. R. N. Katz
Army Materials & Mechanics
Research Center
Watertown, MA 02171

Dr. H. Kirchner
Ceramic Finishing Company
P.O. Box 498
State College, PA 16801

Dr. B. Koepke
Honeywell, Inc.
Corporate Research Center
500 Washington Avenue, South
Hopkins, MN 55343

Mr. Frank Koubek
Naval Surface Weapons Center
White Oak Laboratory
Silver Spring, MD 20910

Dr. F. F. Lange
Westinghouse Electric Corporation
Research Laboratories
Pittsburgh, PA 15235

Dr. J. Lankford
Southwest Research Institute
8500 Culebra Road
San Antonio, TX 78284

Dr. B. R. Lawn
Physics Department
University New South Wales
Kingston, New South Wales
AUSTRALIA

State University of New York
College of Ceramics at Alfred University
ATTN: Library
Alfrd, NY 14802

Dr. R. E. Loehman
University of Florida
Ceramics Division
Gainesville, FL 32601

Dr. N. MacMillan
Materials Research Laboratory
Pennsylvania State University
College Park, PA 16802

Mr. F. Markarian
Naval Weapons Center
China Lake, CA 93555

Dr. F. A. McClintock
Massachusetts Institute of Technology
Department of Mechanical Engineering
Cambridge, MA 02139

Dr. Perry A. Miles
Raytheon Company
Research Division
28 Seyon Street
Waltham, MA 02154

Dr. D. Mulville
Office of Naval Research
Code 474
800 N. Quincy Street
Arlington, VA 22217

Dr. N. Perrone
Office of Naval Research
Code 474
800 N. Quincy Street
Arlington, VA 22217

Dr. J. R. Rice
Brown University
Division of Engineering
Providence, RI 02912

Dr. R. Rice
Naval Research Laboratory
Code 6360
Washington, DC 20375

SUPPLEMENTARY DISTRIBUTION LIST (Cont"d)

Professor R. Roy
Pen sylvania State University
Materials Research Laboratory
Univeristy Park, PA 16802

Dr. L. Rubin
Aerospace Corporation
P.O. Box 92957
Los Angeles, CA 90009

Dr. G. Schmidt
Air Force Materials Laboratory
Wright-Patterson AFB
Dayton, OH 54533

Dr. D. A. Shockey
Stanford Research Institute
Poulter Laboratory
Menlo Park, CA 94025

Dr. R. A. Tanzilli
General Electric Company
Reentry and Environmental Systems Division
3198 Chestnut Street
Philadelphia, PA 19101

Dr. T. Vasilos
AVCO Corporation
Research and Advanced Development Division
201 Lowell Street
Wilmington, MA 01887

Dr. S. M. Wiederhorn
Inorganic Materials Division
National Bureau of Standards
Washington, DC 20234

Dr. N. Corney
Ministry of Defence
The Adelphi
John Adam Street
London WC2N 6BB
UNITED KINGDOM

Professor John Field
University of Cambridge
New Cavendish Laboratory
Cambridge,
UNITED KINGDOM

Dr. L. M. Gillin
Aeronautical Research Laboratory
P.O. Box 4331
Fisherman's Bend
Melbourne, VIC 3001
AUSTRALIA

Dr. B. R. Lawn
Physics Department
University New South Wales
Kingston, New South Wales
AUSTRALIA

UNCLASSIFIED

SECURITY CLASSIFICATION OF THIS PAGE (When Data Entered)

REPORT DOCUMENTATION PAGE		READ INSTRUCTIONS BEFORE COMPLETING FORM
1. REPORT NUMBER	2. GOVT ACCESSION NO.	3. RECIPIENT'S CATALOG NUMBER
4. TITLE (and Subtitle) Study of Erosion Mechanisms of Engineering Ceramics		5. TYPE OF REPORT & PERIOD COVERED Fifth Interim Technical Report (1/1/76 to 3/31/77) 6. PERFORMING ORG. REPORT NUMBER RDR 1778-7
7. AUTHOR(s) Mary Ellen Gulden		8. CONTRACT OR GRANT NUMBER(s) N00014-73-C-0401
9. PERFORMING ORGANIZATION NAME AND ADDRESS Solar, an International Harvester Group PO Box 80966 San Diego, CA 92138		10. PROGRAM ELEMENT, PROJECT, TASK AREA & WORK UNIT NUMBERS NR032-542
11. CONTROLLING OFFICE NAME AND ADDRESS Department of the Navy Office of Naval Research Arlington, VA 22217		12. REPORT DATE April 1977 13. NUMBER OF PAGES 23
14. MONITORING AGENCY NAME & ADDRESS(if different from Controlling Office)		15. SECURITY CLASS. (of this report) Unclassified 15a. DECLASSIFICATION/DOWNGRADING SCHEDULE

16. DISTRIBUTION STATEMENT (of this Report)

Distribution of this document is unlimited.

17. DISTRIBUTION STATEMENT (of the abstract entered in Block 20, if different from Report)

18. SUPPLEMENTARY NOTES

19. KEY WORDS (Continue on reverse side if necessary and identify by block number)

Ceramics	Bend Strength
Erosion	Particle Mass
Silicon Nitride	Particle Velocity

20. ABSTRACT (Continue on reverse side if necessary and identify by block number)

Erosion behavior of hot pressed and reaction bonded Si_3N_4 was determined using natural quartz particles in the subsonic velocity regime. Six narrow size ranges were used varying between 15 and 385μm average diameter. Erosion behavior of these two forms of Si_3N_4 was markedly different. It was found that erosion of hot pressed Si_3N_4 was proportional to particle momentum (mass x velocity) over five orders of

DD FORM 1 JAN 73 1473 EDITION OF 1 NOV 65 IS OBSOLETE

UNCLASSIFIED

SECURITY CLASSIFICATION OF THIS PAGE (When Data Entered)

magnitude. Erosion of reaction bonded silicon nitride was approximately proportional to the fourth order of both particle size and velocity. Strength of hot pressed Si_3N_4 was not reduced under these test conditions. However, a major strength decrease was exhibited by the reaction bonded material. Examination revealed that erosion or impact of these materials under these test conditions did not clearly fit the current models for brittle materials, and that more than one mechanism exists. A small test program was performed on a MgF_2 target impacted with large SiC particles used as an additive in some aircraft carrier decking. It was found that cracking and material loss was sustained by the target at velocities as low as 15 mps.